Implementing a New Dose-response Model for Estimating Infection Probability of Campylobacter Jejuni based on the Key Events Dose-response Framework

Hiroki Abe
Hokkaido University
Kohei Takeoka
Hokkaido University
Yuto Fuchisawa
Hokkaido University
Kento Koyama
Hokkaido University
Shigenobu Koseki (koseki@bpe.agr.hokudai.ac.jp)
Hokkaido University

Research Article

Keywords: ingested pathogenic bacteria, foodborne pathogens, mechanistic , uman gastrointestinal environment

Posted Date: January 25th, 2021

DOI: https://doi.org/10.21203/rs.3.rs-148212/v1

Version of Record: A version of this preprint was published at Applied and Environmental Microbiology on September 28th, 2021. See the published version at https://doi.org/10.1128/AEM.01299-21.

Implementing a new dose-response model for estimating infection probability of *Campylobacter jejuni* based on the key events dose-response framework

Hiroki Abe, Kohei Takeoka, Yuto Fuchisawa, Kento Koyama, Shigenobu Koseki*

Graduate School of Agricultural Science, Hokkaido University, Kita-9, Nishi-9, Kita-ku, Sapporo 060-8589, Japan

*Corresponding author: Phone/fax: +81 11 706 2552

E-mail address: koseki@bpe.agr.hokudai.ac.jp (S. Koseki)

Abstract

Understanding the dose-response relationship between ingested pathogenic bacteria and infection probability is a key factor for appropriate risk assessment of foodborne pathogens. The objectives of this study were to develop and validate a novel mechanistic dose-response model for *Campylobacter jejuni* and simulate the underlying mechanism of foodborne illness during digestion. Bacterial behavior in the human gastrointestinal environment, including gastric reductions, transition to intestines, and invasion to intestinal tissues, was described using a Bayesian statistical model based on the reported experimental results of each process while considering physical food types (liquid or solid) and host age (young or elderly). Combining the models in each process, the relationship between pathogen intake and the cell invasion probability of *C. jejuni* was estimated and compared with reported epidemiological dose-response relationships. Taking food types into account, estimations of the cell invasion probability of *C. jejuni* successfully described the reported dose-response relationships from substantial accidents. The developed calculation framework is thus potentially applicable to other pathogens to quantify the dose-response relationship from experimental data obtained from digestion.

Introduction

Dose-response models play an important role in quantitative microbial risk assessment (QMRA) for food. While the exposure assessment of the QMRA helps predict the bacterial response during processing and distribution of foods, dose-response models play a key role in risk characterization, which estimates the probability of illness or infection from pathogen intake counts derived from the exposure assessment. Three main approaches for developing dose-response relationships of foodborne pathogens are available: testing with human volunteers, animal tests, and epidemiological estimation from outbreak data. Although each approach has strengths and limitations, all three approaches have substantial uncertainty owing to the inherent variability in the pathogen, host, and food vehicle. In addition, it is generally difficult to collect data at a low pathogen concentration to which a person is exposed, and it is difficult to collect relevant data during the response [1].

An alternative approach has been suggested for establishing dose-response models; the Key Events Dose-Response Framework (KEDRF) [2]. KEDRF is an approach based on important infection mechanisms causing foodborne illness, called key events, and available data from digestive systems to gain insight into dose-response relationships. As the method for estimating the dose-response relationship is based on infection mechanisms, KEDRF is expected to have several advantages, such as potential of responding to low-dose infection, considering host health, sex, pathogen strain, and variability.

Few studies have focused on developing dose-response models based on infection mechanisms or key event models describing pathogen response in humans. Koseki et al. [3] and Takeoka et al. (in submission) developed key event models that dynamically describe

50 the death of some pathogens in simulated gastric fluid mimicking stomach digestion. Pujol
51 et al. [4] described immune capacities until the occurrence of infection. Pathogens, such as
52 *Listeria*, *Salmonella*, and *Campylobacter,* adhere to and invade intestinal epithelial cells
53 and cause disease [5]. Caco-2 cells are commonly used to observe the adhesion and invasion
54 of pathogens to intestinal epithelial cells *in vitro*. We recently developed a model
55 describing the invasion kinetics of pathogens in human intestinal cells [6]. Although one
56 study has previously estimated the dose-response relationship of *Listeria* through
57 mathematical modeling of bacterial colonization in the human intestine after reductions in
58 the human stomach [7], this mechanistic dose-response model does not consider cell invasion
59 by the pathogen in terms of infection and that pathogen colonization in the intestines does
60 not always cause infection. The final dose-response relationship needs to describe illness
61 and modeling competitions with the immune system after the invasion of tissues by
62 pathogens and the onset of illness. In these respects, KEDRF is still a developing concept.
63 It is desirable to develop a more sophisticated key events dose-response model to further
64 elucidate the reality of foodborne illness.
65 It is necessary to incorporate the concept of bioaccessibility in KEDRF to develop a
66 more sophisticated mechanistic dose-response model. The term “bioaccessibility,” along
67 with “bioavailability,” is a key concept to ascertain nutritional efficiency of food and food
68 formulas developed to improve human health in terms of pharmacokinetics and nutrition [8].
69 Bioaccessibility is defined as the number of chemicals or nutrients that are released from
70 the gastrointestinal tract tissue, which are made available through blood vessels via
71 absorption. It is evaluated using in vitro digestion models, generally simulating gastric or

small intestinal digestion, as revealed through a Caco-2 cell uptake test [9]. Infectious foodborne pathogens invade the tissues through the stomach and intestines, causing inflammation in the gastrointestinal tract, or travel to the affected area, such as blood or lymph, and cause symptoms. Pathogens also trigger physiological reactions through the same pathways as nutrients and chemicals (perhaps slightly oversimplified). At present, it is difficult to experimentally replicate and model the competition between pathogens and immune cells, but the pathways for invading intestinal tissues have been reproduced in vitro. Assessing the bioaccessibility of pathogens is essential to assume a dose-response relationship with KEDRF as a reference.

This study aimed to develop an alternative dose-response model of *Campylobacter jejuni*, which is one of the most dangerous pathogenic bacteria, based on KEDRF, considering food type and host age. We estimated the invasion probability, defined as the probability of infection, accounting for food type in the gastric retention time and age in the gastric pH. The estimated infection probability was compared and validated using actual epidemiological data.

Results

Gastric bacterial reduction

Changes in the pH of young and elderly individuals could be successfully described using an exponential model (Fig. 2). All the estimated parameters of the exponential model were convergent for pH changes after liquid and solid meals among young and elderly individuals (Supplementary Fig. S2) because the Gelman-Rubin convergence statistic (R-hut value) of parameter distributions was 1.0. The estimation of the fitted exponential

model indicated that the changes in the pH in the stomachs of elderly individuals were broader than those of young individuals (Fig. 2). Differences in the reduction behavior of *C. jejuni* were shown to be due to differences in pH (Fig. 3). The calculated survival ratio of elderly individuals after ingestion of liquid and solid foods was higher than that of the calculated survival transit ratio of young individuals.

Bacterial transfer to the small intestine

The changes in the retention ratio in the stomach for solids and liquids could be successfully described as a cumulative gamma distribution (Fig. 4). Estimated parameter distributions converged with Bayesian inference because all R-hut values of parameter distributions were 1.0 (Supplementary Fig. S3). The mean (± standard deviation) time of estimated gastric retention of solid foods was 1.5 ± 0.52 h, and the mean of estimated gastric retention of liquid foods was 0.77 ± 0.84 h. The survival ratio of intestinal transit varied with food type and age (Fig. 5). There was a significant difference in the survival transit ratio in young and elderly people after eating solid food. While, there was not notably difference between survival transit ratio of young and elderly individuals after eating liquid foods (Fig. 5 a and b). In addition, considering food type difference, there was a difference in the estimated survival pathogen transit ratio regardless of age (Fig. 5).

Retention time in the small intestine

The changes in the colonic filling ratio could be successfully described as a cumulative gamma distribution (Fig. 6). The estimated parameter distributions converged with

116 Bayesian inference since all R-hut values of parameter distributions were 1.0
117 (Supplementary Fig. S4). The mean time of estimated intestinal retention was 5.8 ± 2.0 h.
118
119 **Probability of infection in human intestinal cells**
120 The estimated cell invasion probability of *C. jejuni* varied with food type and age (Fig. 7).
121 There were no differences in the prediction of infection probability among the strains
122 (Supplementary Fig. S7, S8, and S9). The prediction of the infection probability of all three
123 *C. jejuni* strains is shown in Fig. 7. Young and elderly individuals consuming liquid food
124 (liquid-young and liquid-elderly, respectively), as well as elderly individuals consuming
125 solid food (solid-elderly) estimated infection probabilities were similar to the reported
126 dose-response relationships with bovine milk [10], and all three strains' 95% prediction bands
127 covered the reported dose-response relationship. The root mean square error (RMSE) of the
128 median prediction of young-liquid, elderly-solid, and elderly-liquid groups were 0.69, 0.84,
129 and 0.21 log CFU, respectively, when the logarithms of pathogen dose were assumed as
130 objective variables. In contrast, the RMSE of the median prediction of the young-solid
131 group was 1.2 log CFU and the 95% prediction band did not cover the reported dose-
132 response relationship.
133
134 **Sensitivity analysis of the framework for estimating invasion probability**
135 Figure 8 shows the Spearman's rank correlation coefficients of model components (e.g.,
136 food type, model parameters, $N_{intestine}$, and $t_{intestinal}$) against the infection probability.

The upper factors in Fig. 8 were more relevant to the estimated infection probability. The indicators of liquid and solid food were set as 0 and 1, respectively, and the indicators of the strains were set as follows: RIMD 0366027, 1; RIMD 0366042, 2; and RIMD 0366048, 3. The indicators for age were set as the mean age of individuals subjected to the pH test (young: 25; elderly: 71). The most relevant factor against the infection probability was the cell-invading pathogen count (R: 0.96; p-value < 10^{-6}). The second position of the relevant factor was the logarithm of pathogen count intake (R: 0.90; p-value < 10^{-6}). Since the infection probability was directly derived from these two factors, it is natural that these factors have the most relevance. The third position of the relevant factor was the intestinal survival ratio (R: 0.29; p-value < 10^{-6}). The relevant factors from the first to the third place were computable. The most important factors in the parametric factors were the shape parameter of the gamma distribution for gastric retention (R: -0.23; p-value < 10^{-6}), the second factor was the scale parameter of the gamma distribution for gastric retention (R: -0.23; p-value < 10^{-6}), and the third factor was food type (R: -0.23; p-value < 10^{-6}). The factors with a p-value more than 0.05 were intestinal retention α (p-value: 0.06), intestinal retention β (p-value: 0.11), stomach reduction b (p-value: 0.39), intestinal retention time (p-value: 0.70), invasion ratio (p-value: 0.70), invasion $LogN_{max}$ (p-value: 0.96), and strain (p-value: 0.99).

Discussion

Here, this study aimed to develop an alternative dose-response model of *C. jejuni*, one of the most dangerous pathogenic bacteria, through KEDRF, considering food type and host age. Despite the completely different approach to estimating the dose-response relationship using conventional methods, the predictive model developed in this study successfully predicted the reported illness probability of campylobacteriosis [10]. The reported dose-response relationship (illness probability) resulted from contaminated milk consumption, which could be properly predicted from among predictions of the KEDRF dose-response model for both young and elderly individuals ingesting liquid foods. However, it should be noted that there were small but unignorable RMSEs of young and elderly individuals ingesting liquid foods (0.69 and 0.84 log CFU, respectively) with a reported dose-response relationship. The infection probability according to the dose-response relationship estimated in this study was based on the probability of invasion into intestinal cells. Because the immune system prevents symptoms of the illness after the invasion of the intestinal tissue, the illness probability being lower than the infection probability is natural.

The predicted results of this study showed that *C. jejuni* could invade the intestinal tissues and infect the human body even at a dose as low as 1–10 CFU. The previously reported epidemiological data on milk consumption also exhibited the occurrence of the disease at low doses. In contrast, the dose-response of *C. jejuni* demonstrated herein showed a discrepancy with the previously reported model [11], which is also the most widely used dose-response relationship for *C. jejuni* in QMRA. The infection probability reported

by Black et al. [11] was based on the presence of *C. jejuni* in stools, the definition of which was completely different from that examined in this study. The difference in definition might be the reason for the difference in the prediction results. It has been reported that *C. jejuni* growth is inhibited upon competition with the extended-spectrum β-lactamase-producing bacteria, including some strains of *Escherichia coli*, which are widespread in nature [12]. In the colon, which is not an optimum environment for *C. jejuni* because of the anaerobic environment, the number of viable *C. jejuni* may decrease owing to competition with other intestinal bacteria. *C. jejuni* may be reduced before it is detected in the stool owing to competition for nutrients or competitive effects in the gut, such as the Jameson effect [13]. Considering the actual behavior of *C. jejuni* in the human body, it is better to discuss the illness probability or the invasion probability into human tissues, which is the definition used for the probability of infection in this study.

While the results for the prediction were similar to those reported for actual dose-response relationships[10], it was also possible to show the effectiveness of the implementation of the computational framework based on KEDRF. In particular, the results will be considered very beneficial, because the dose-response relationship depends on the food type and the age of the host. The FAO/WHO risk assessment for *Listeria* also emphasizes the importance of dose-response relationships in elderly and high-risk populations [14]. In particular, the results of this study indicated a large difference in the infection probability (Young: 1.9 log CFU; Elderly: 1.1 log CFU) among the food types. In the sensitivity analysis, the factor related to the retention time in the stomach had the largest correlation among the parameters. Figure 5 shows that when consuming liquid food, the

number of *C. jejuni* reaching the intestines was higher than that when consuming solid food owing to the difference in the gastric retention time. The difference in the predicted probability of infection between solid and liquid foods was due to the difference in the gastric retention time. In contrast, the predictions did not show any difference among pathogen strains. In the present dose-response model, the strains were reflected only in the invasion into the intestinal tissue. Although there was no strain difference in the invasion behavior, there could be differences in some other key events, such as survival in the stomach. KEDRF has the potential to estimate the probability of infection in young children since the difference between the elderly and young individuals was considered in this study. KEDRF, which can simultaneously consider various conditions, such as host and food type, would be a useful tool for estimating dose-response relationships.

Key event models using Bayesian inference are important in KEDRF, where predictions are chained for each key event. This study attempted to illustrate the variability and uncertainty of pathogen behavior and the environment of the gastrointestinal tract based on Bayesian inference. Modeling using Bayesian inference has been used to describe various bacterial behaviors, such as the growth and death of various bacteria, as a method that can represent variability and uncertainty [6,15-17]. In addition, KEDRF suggests that modeling the individual variability of the digestive process in different hosts will lead to a better understanding of food poisoning incidents. The use of Bayesian inference to represent not only bacterial but also host variability will allow the estimation of appropriate dose-response relationships using mechanistic approaches.

222 Although this study has shown that KEDRF is a useful procedure for predicting
223 dose-response relationships of *C. jejuni*, KEDRF is also effective for other types of
224 bacteria. The approach used in this study consisted of a mathematical prediction model
225 based on predictive microbiology and pharmacokinetics. The growth and death of *C. jejuni,*
226 as well as various other pathogens, were described using predictive models. For many other
227 pathogens, the present method can be applied to calculate the intestinal viable bacterial
228 count using gastric retention time and survival kinetics in the stomach, independent of the
229 pathogen type. Development of dose-response models based on KEDRF is expected for
230 various foodborne pathogens.
231 However, the dose-response model based on KEDRF presented in this study still
232 has certain limitations. The present study did not consider the growth of *C. jejuni* in the
233 intestines because its growth rate is slower than its invasion rate [6]. In contrast, a growth
234 model is needed for fast-growing pathogenic bacteria, such as *E. coli* or *Salmonella*.
235 Modeling the interactions between the immune system and pathogens is also required. It
236 has been suggested that the probability of infection may be high, but the illness may not
237 develop [18]. Modeling the effect of immunity on pathogens will be necessary to predict the
238 probability of illness. Furthermore, since the available data on the gastrointestinal tract
239 were limited, the effect of age was reflected only in the pH change and the effect of food
240 type was reflected only in the residence time in the stomach in this study. However, for a
241 more realistic prediction, data corresponding to age and food types in all gastrointestinal
242 environments, such as pH change, gastric retention time, and intestinal retention time, are
243 needed. For more realistic and appropriate predictions of the dose-response relationship

244 based on KEDRF, it is necessary to study immune modeling and additional environmental
245 data of the gastrointestinal tract under various conditions.
246 In conclusion, the behavior of *C. jejuni* in the gastrointestinal tract based on the
247 KEDRF was successfully predicted via mathematical models using Bayesian inference.
248 Moreover, the respective dose-response relationships for combinations of age (young,
249 elderly) and food type (liquid, solid) were also estimated. The results of the dose-response
250 model of KEDRF showed similar results to the reported dose-response relationship.
251 Furthermore, sensitivity analysis of the prediction results showed that gastric retention time
252 was the most relevant factor among the key events from ingestion to invasion. This study
253 demonstrated a large potential for the development of a novel dose-response model based
254 on KEDRF. The dose-response model based on KEDRF will allow us to estimate the dose-
255 response relationships of various pathogens with various factors, such as age, sex, chronic
256 illness, food type, and others based on their actual infection mechanisms.
257
258 **Methods**
259 **Determining the key events of campylobacteriosis infection**
260 The key events of the infection mechanism were ascertained on the basis of the KEDRF
261 report [1]. Since it is difficult to quantitatively assess pathogens in the human body, this study
262 considered the probability of invasion into the small intestinal endothelial cells as the
263 infection probability. The following were identified as key events: (i) pathogen reduction in
264 the stomach; (ii) transfer to the small intestine from the stomach; (iii) pathogen invasion
265 into small intestinal epithelial cells. The growth of *C. jejuni* in the small intestine was not

266 considered because a preliminary test indicated that it was relatively slow compared to the
267 invasion rate of the epithelial cells [6]. Figure 1 shows the constructed model, and the
268 abbreviations are summarized in Supplementary Table S1. All the computations were
269 calculated under the Anaconda distribution (Python 3.7.7) (See data availability section).
270
271 **Modeling for postprandial gastric pH change among younger and elder individuals**
272 The postprandial pH changes among young and elderly individuals were expressed
273 separately in a mathematical model. The exponential models (Eq. 1) were fitted to the
274 reported pH changes after a standard meal (1000 kcal) for young [19] and elderly individuals
275 [20]:
276 $$pH_{(t)} = pH_0 e^{-k_{pH}t} + pH_{min} \quad (1),$$
277 where $pH_{(t)}$ denotes the pH at a time after food intake, t; pH_0 denotes pH immediately
278 after a meal; k_{pH} denotes the decreasing rate of pH; pH_{min} denotes the convergence value
279 of pH. The parameters were estimated using Bayesian inference through pystan (ver. 2.19.).
280 The normal distribution, which is generally used, was adopted as the prior distribution of
281 pH, as distributions of the reported data were contrasting.
282
283 **Pathogen survival in stomach with between- and within-strain variability**
284 The survival of *C. jejuni* was described using a previously reported dynamic survival model
285 of *C. jejuni* (Eq. 2) under artificial gastric conditions using Bayesian inference (Takeoka et
286 al., in submission). The between- and within-strain variability reduction model was
287 constructed from the data of 11 strains of *C. jejuni* (RIMD 0366026, RIMD 0366027,

RIMD 0366028, RIMD 0366029, RIMD 0366042, RIMD 0366043, RIMD 0366044, RIMD 0366048, RIMD 0366049, RIMD 0366050, and RIMD 0366051).

$$log_{10} S_{g(t+\Delta t)} = -\left(\frac{t^*+\Delta t}{\delta_{(\overline{pH})}}\right)^{p_{(\overline{pH})}} \quad (2.\ a)$$

$$t^* = \delta_{(\overline{pH})}\left(-log_{10} S_{g(t)}\right)^{\frac{1}{p}}$$

$$\begin{cases} ln(\delta_{(\overline{pH})}) = a \times pH + b \\ ln(p_{(\overline{pH})}) = e \times pH + f \end{cases} \quad (2.\ b)$$

$$\begin{pmatrix} a \\ b \\ e \\ f \end{pmatrix} \sim MultiNormal\_Cholesky\left(\begin{pmatrix} a_0 \\ b_0 \\ e_0 \\ f_0 \end{pmatrix}, \Sigma_{chol}\right) \quad (2.\ c)$$

where $S_{g(t)}$ denotes the bacterial survival ratio defined as the ratio of the surviving bacterial counts divided by the initial bacterial counts; p denotes the power parameter of the Weibull model; δ denotes the time of the first decimal reduction of the Weibull model; and $\overline{pH}$ denotes the mean pH during the time intervals from t to $t + \Delta t$ as $\overline{pH} = \frac{pH_{(t)}+pH_{(t+\Delta t)}}{2}$. The parameters of the primary model, δ and p, were defined using the parameters of the secondary model (a, b, c, f), following the multivariate normal distribution of Cholesky parameterization, in which Σ_{chol} is the Cholesky factor of the covariance matrix of $log(p_{(\overline{pH})})$ and $log(\delta_{(\overline{pH})})$ of all strains.

Bacterial transfer to the small intestine

Changes in the gastric retention ratio were described as the cumulative gamma distribution, which is used to describe the waiting time of traffic jams and transmitting times. Comparing the transfer time of solid foods and liquid foods, the effect on the cell invasion ability due to differences in food type was estimated. The changes in gastric retention ratio were described using the following cumulative gamma distribution fitted to the reported change in the gastric retention ratio after solid and liquid meals: [21]

$$R_g = 1 - \frac{1}{\Gamma_{(\alpha)}}\gamma_{(\alpha,\beta t)} \quad (3),$$

where R_g is the gastric retention ratio; α is the shape parameter; β is the rate parameter of gamma distribution; $\Gamma_{(\alpha)}$ is the gamma function $\Gamma_{(\alpha)} = \int_0^\infty e^{-u}u^{\alpha-1}\,du$; $\gamma_{(\alpha,\beta t)}$ is the lower incomplete gamma function $\gamma_{(\alpha,\beta t)} = \sum_{k=0}^{\infty}\frac{(\beta t)^{\alpha+k}e^{-\beta t}}{\alpha(\alpha+1)\ldots(\alpha+k)}$.

The combined equation of pH, pathogenic survival, and gastric retention model, as well as the ratio of the surviving pathogen transfer to the intestine, $r_{intestine}$, was described (Eq. 4; graphically description: Supplementary Fig. S1), and discretely expressed as shown in Eq. 4.b:

$$r_{intestine,(t)} = \int_0^t S_{g(s)}\frac{dR_g}{ds}\,ds \quad (4.\ a)$$

$$r_{intestine,(t_k)} = \sum_{i=1}^{k}\frac{S_{(t_i)}}{n} \quad (4.\ b)$$

where s denotes an operator; t_i denotes the simulated gastric retention times from the gamma distributions; n denotes the total simulation counts from the gamma distributions; k

denotes any natural number between 1 and n. Using Eq. 4, the survival pathogen transit counts, $N_{intestinal}$, were derived as follows:

$$N_{intestine} = r_{intestine} N_{dose} \quad (5)$$

where N_{dose} denotes the intake counts of pathogens.

Bacterial invasion in intestinal cells

Invasion of *C. jejuni* was described using a modified predictive model based on a previously reported *C. jejuni* model [6] (RIMD 0366027, RIMD 0366042, and RIMD 0366048) applying invasion count, $N_{invading}$, to Caco-2 cells as follows:

$$\frac{d}{dt} N_{invading} = \mu \frac{N_{exposure} - N_{invading}}{V} \left(S N_{max} - N_{invading} \right) \quad (6)$$

where μ, $N_{exposure}$, N_{max}, V, and S denote the cell invasion rate, the pathogen exposure count, the spatial maximum invading pathogen count per 1 cm^2, the volume of intestinal juice (319 mL) [22] and the surface area of the small intestine (32 m^2), respectively [23].

Retention time in the small intestine

The cumulative gamma distribution was fitted to the change in the small intestinal retention ratio, $R_{intestinal}$, as the reported colonic filling ratio was as follows [24]:

$$R_{intestinal} = 1 - \frac{1}{\Gamma_{(\alpha)}} \gamma_{(\alpha', \beta' t)} \quad (7)$$

Considering Eq. 7, small intestinal retention time, $t_{intestinal}$, follows the gamma distribution α' as a shape parameter and β' as a rate parameter; $Gamma(\alpha', \beta')$ as follows:

$$t_{intestinal} \sim Gamma(\alpha', \beta') \quad (8)$$

Invasion probability in human tissues

The probability of pathogen invasion into the cells was determined as previously described [6]. One or more *C. jejuni* cell invasion probabilities were derived from the models as follows:

$$P_{invading} = 1 - \left(1 - \frac{N_{invading\,(t_{intestinal})}}{N_{Dose}}\right)^{N_{Dose}} \quad (9)$$

Spearman's rank correlation coefficients between $P_{invading}$ and the parameters were established as a sensitivity analysis of the current dose-response model.

References

1. Buchanan, R. L., Havelaar, A. H., Smith, M. A., Whiting, R. C. & Julien, E. The key events dose-response framework: its potential for application to foodborne pathogenic microorganisms. *Crit. Rev. Food Sci. Nutr.* **49**(8)**,** 718–728 (2009).
2. Julien, E., Boobis, A. R., Olin, S. S. & Ilsi Research Foundation Threshold Working Group. The key events dose-response framework: a cross-disciplinary mode-of-action based approach to examining dose-response and thresholds. *Crit. Rev. Food Sci. Nutr.* **49**(8)**,** 682–689 (2009).
3. Koseki, S., Mizuno, Y. & Sotome, I. Modeling of pathogen survival during simulated gastric digestion. *Appl. Environ. Microbiol.* **77**(3)**,** 1021–1032 (2011).
4. Pujol, J. M., Eisenberg, J. E., Haas, C. N. & Koopman, J. S. The effect of ongoing exposure dynamics in dose response relationships. *PLOS Comput. Biol.* **5**(6)**,** e1000399; 10.1371/journal.pcbi.1000399 (2009).
5. Ribet, D. & Cossart, P. How bacterial pathogens colonize their hosts and invade deeper tissues. *Microbes Infect.* **17**(3)**,** 173–183 (2015).
6. Abe, H., Koyama, K. & Koseki, S. Modeling invasion of Campylobacter jejuni into human small intestinal epithelial-like cells by Bayesian inference. *Appl. Environ. Microbiol.* **87**(1)**,** e01551-20; 10.1128/AEM.01551-20 (2020).
7. Rahman, A., Munther, D., Fazil, A., Smith, B. & Wu, J. Advancing risk assessment: mechanistic dose–response modelling of Listeria monocytogenes infection in human populations. *R. Soc. Open Sci.* **5**(8), 180343; 10.1098/rsos.180343 (2018).
8. Fernández-García, E., Carvajal-Lérida, I. & Pérez-Gálvez, A. In vitro bioaccessibility assessment as a prediction tool of nutritional efficiency. *Nutr. Res.* **29**(11)**,** 751–760 (2009).
9. Galanakis, C. M. *Nutraceutical and Functional Food Components* (Academic Press, 2016)

10. Teunis, P. *et al.* A reconsideration of the *Campylobacter* dose–response relation. *Epidemiol. Infect.* **133**(4)**,** 583–592 (2005).

11. Black, R. E., Levine, M. M., Clements, M. L., Hughes, T. P. & Blaser, M. J. Experimental Campylobacter jejuni infection in humans. *J. Infect. Dis.* **157**(3)**,** 472–479 (1988).

12. Hazeleger, W. C., Jacobs-Reitsma, W. F. & den Besten, H. M. W. Quantification of Growth of Campylobacter and extended spectrum β-lactamase producing bacteria sheds light on black box of enrichment procedures. *Front. Microbiol.* **7**, 1430; 10.3389/fmicb.2016.01430 (2016).

13. Jameson, J. E. A discussion of the dynamics of salmonella enrichment. *J. Hyg. (Lond).* **60,** 193–207 (1962).

14. Food & Agriculture Organization. *Risk Assessment of Listeria monocytogenes in Ready-to-Eat Foods*, 2004

15. Koyama, K., Aspridou, Z., Koseki, S. & Koutsoumanis, K. Describing uncertainty in salmonella thermal inactivation using Bayesian statistical modeling. *Front. Microbiol.* **10,** 2239; 10.3389/fmicb.2019.02239 (2019).

16. Huang, L. & Li, C. Growth of Clostridium perfringens in cooked chicken during cooling: one-step dynamic inverse analysis, sensitivity analysis, and Markov chain Monte Carlo simulation. *Food Microbiol.* **85,** 103285; 10.1016/j.fm.2019.103285 (2020).

17. Garre, A., Zwietering, M. H. & den Besten, H. M. W. Multilevel modelling as a tool to include variability and uncertainty in quantitative microbiology and risk assessment. Thermal inactivation of Listeria monocytogenes as proof of concept. *Food Res. Int.* **137,** 109374; 10.1016/j.foodres.2020.109374 (2020).

18. Teunis, P. F. M., Bonačić Marinović, A., Tribble, D. R., Porter, C. K. & Swart, A. Acute illness from Campylobacter jejuni may require high doses while infection occurs at low

doses. *Epidemics* **24,** 1–20 (2018).

19. Dressman, J. B. *et al.* Upper gastrointestinal (GI) pH in young, healthy men and women. *Pharm. Res.* **7**(7)**,** 756–761 (1990).

20. Russell, T. L. *et al.* Upper gastrointestinal pH in seventy-nine healthy, elderly, North American men and women. *Pharm. Res.* **10**(2)**,** 187–196 (1993).

21. Hellström, P. M., Grybäck, P. & Jacobsson, H. The physiology of gastric emptying. *Best Pract. Res. Clin. Anaesthesiol.* **20**(3)**,** 397–407 (2006).

22. Schiller, C. *et al.* Intestinal fluid volumes and transit of dosage forms as assessed by magnetic resonance imaging. *Aliment. Pharmacol. Ther.* **22**(10)**,** 971–979 (2005).

23. Helander, H. F. & Fändriks, L. Surface area of the digestive tract - revisited. *Scand. J. Gastroenterol.* **49**(6)**,** 681–689 (2014).

24. Read, N. W., Al-Janabi, M. N., Holgate, A. M., Barber, D. C. & Edwards, C. A. Simultaneous measurement of gastric emptying, small bowel residence and colonic filling of a solid meal by the use of the gamma camera. *Gut* **27**(3)**,** 300–308 (1986).

Acknowledgments

This study was supported by a grant from the Food Safety Commission, Cabinet Office, Government of Japan (Research Program for Risk Assessment Study on Food Safety, No. 1802) and a Grant-in-Aid for Japan Society for the Promotion of Science Fellows, Grant number 20J11550).

Author contributions

Competing interests

The author(s) declare no competing interests.

Data availability

The Python codes are available through co-author GitHub (URL: the link will be paste here after the review).

For reviewers link: https://www.dropbox.com/sh/f6tuqo8gx8egglv/AAD-9mic5MYtF76kzNYw11P-a?dl=0

Figure legends

Figure 1. Directed acyclic graph of the model parameters and factors. Solid arrows indicate distributions, dashed arrows deterministic functions. The abbreviations and details of components are summarized in Supplementary Table S1.

Figure 2. Reported after-meal pH changes (points) of young (upper) and elderly (lower) people, and the prediction band derived from the exponential model. (Appendix: the MCMC trace plots of parameters and the estimated parameter distribution of pH model).

Figure 3. Predicted after-meal survival curves (solid curve: median, dash curve and covered range: 90% prediction band) of *C. jejuni* in the stomach of young (upper) and elderly (lower) people.

Figure 4. Reported retention ratio (**a**; points) & predicted cumulative gamma distributions (**a** and **b**; solid curve: median, dash curve and covered range: 95% prediction band) for gastric retention time (Appendix: Estimated parameter distribution of retention models).

Figure 5. Calculated transferred survival ratio (solid curve: median, dash curve and covered range: 90% prediction band) in intestine under each condition (**a**: young and liquid food, **b**: elderly and liquid food, **c**: young and liquid food, **d**: elderly and solid food).

454 Figure 6. Reported colonic filling ratio (**a**; points) and predicted cumulative gamma
455 distribution for retention time in small intestines (**a** and **b**; solid curve: median, dash curve
456 and covered range: 95% prediction band). (Appendix Estimated parameter distribution of
457 colonic filling)
458
459 Figure 7. Cell invasion probability (solid curve: median, dash curve and covered range:
460 60% and 95% prediction band) of *C. jejuni* (total of all three strains) under each condition
461 (Same position as Fig. 5) and the reported dose-response relationship (square; Teunis et al.,
462 2005)
463
464 Figure 8. Spearman's ranked correlation coefficients of parameter and computable factors
465 against the predicted infection probability.

Figures

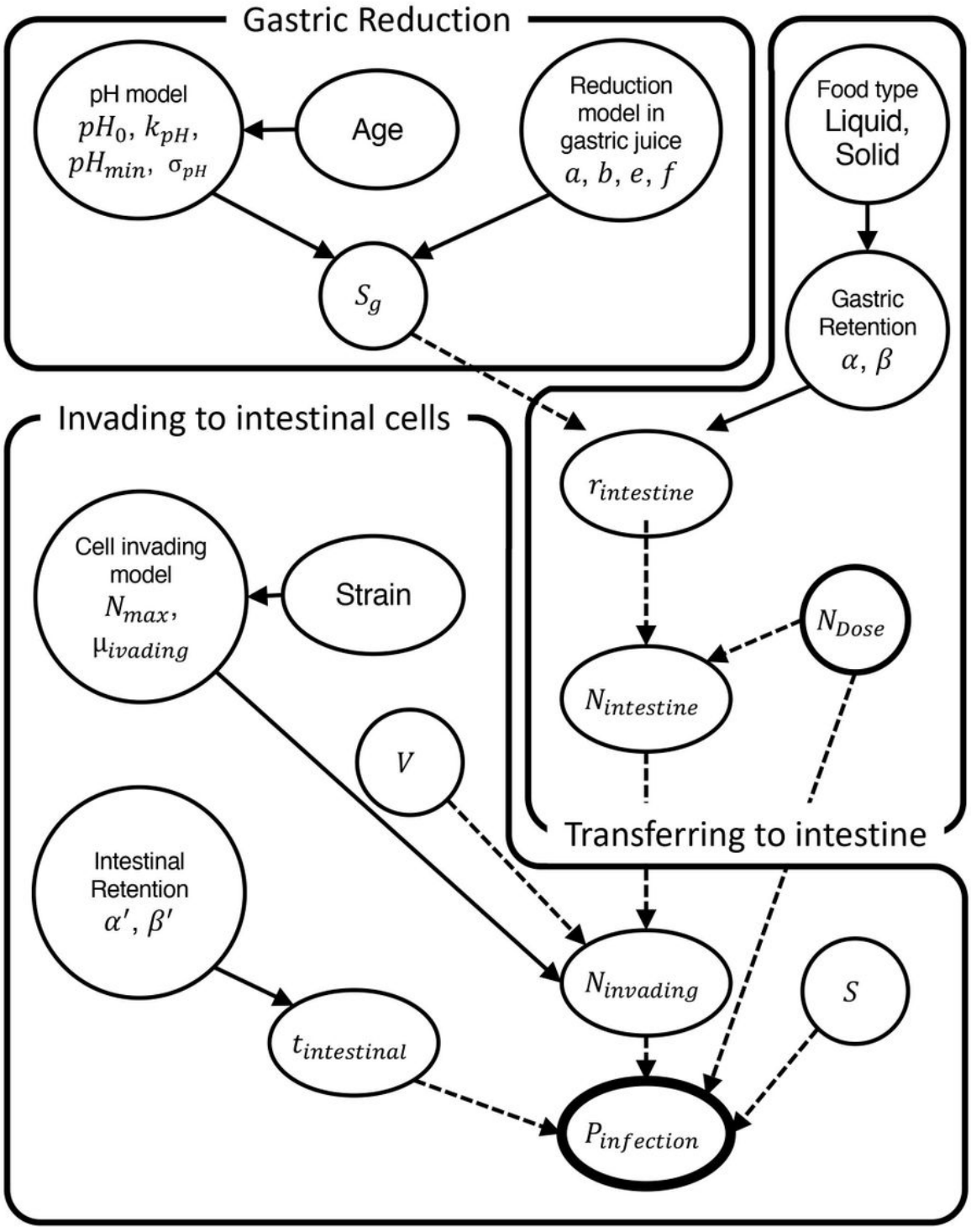

Figure 1

Directed acyclic graph of the model parameters and factors. Solid arrows indicate distributions, dashed arrows deterministic functions. The abbreviations and details of components are summarized in Supplementary Table S1.

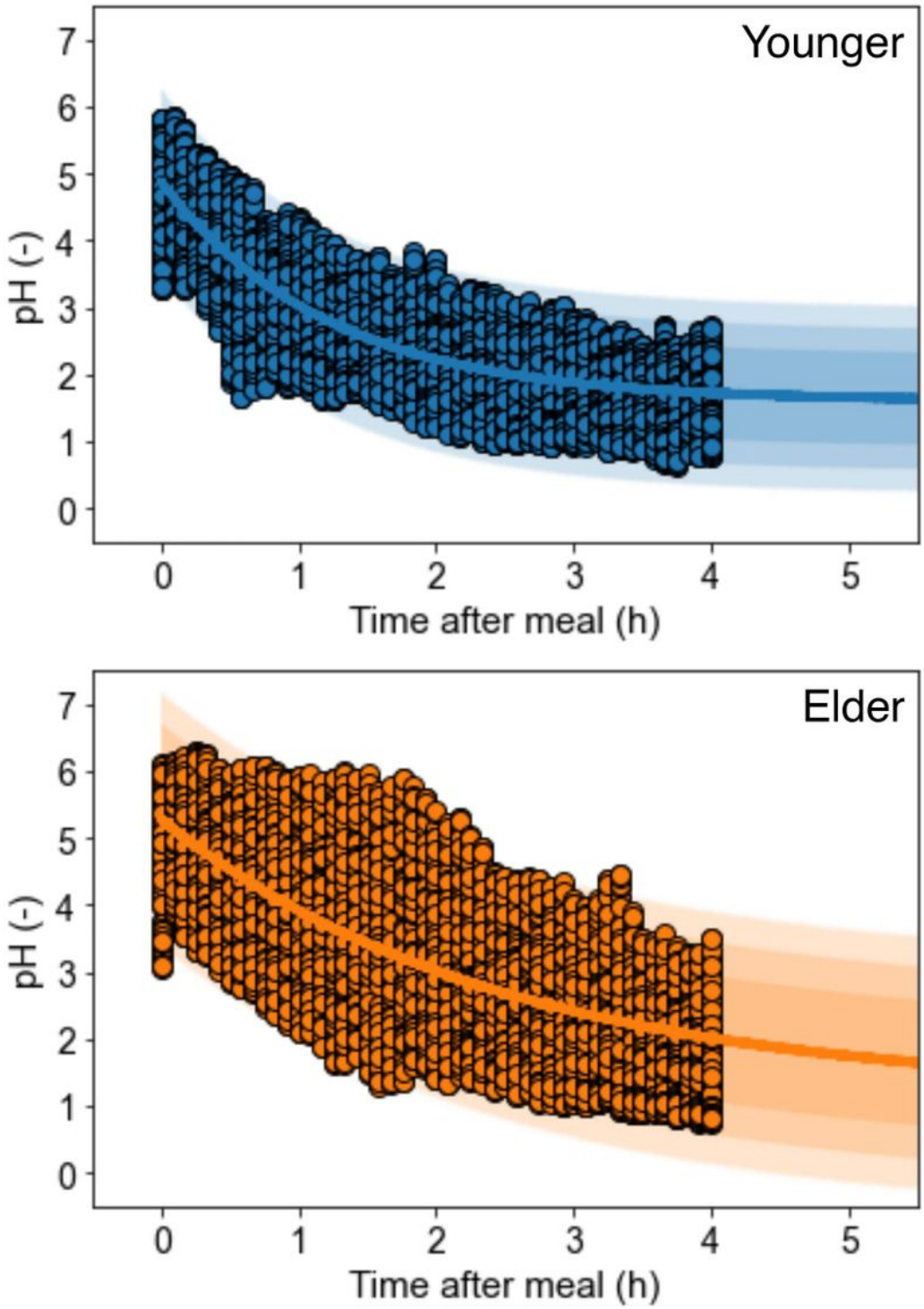

Figure 2

Reported after-meal pH changes (points) of young (upper) and elderly (lower) people, and the prediction band derived from the exponential model. (Appendix: the MCMC trace plots of parameters and the estimated parameter distribution of pH model).

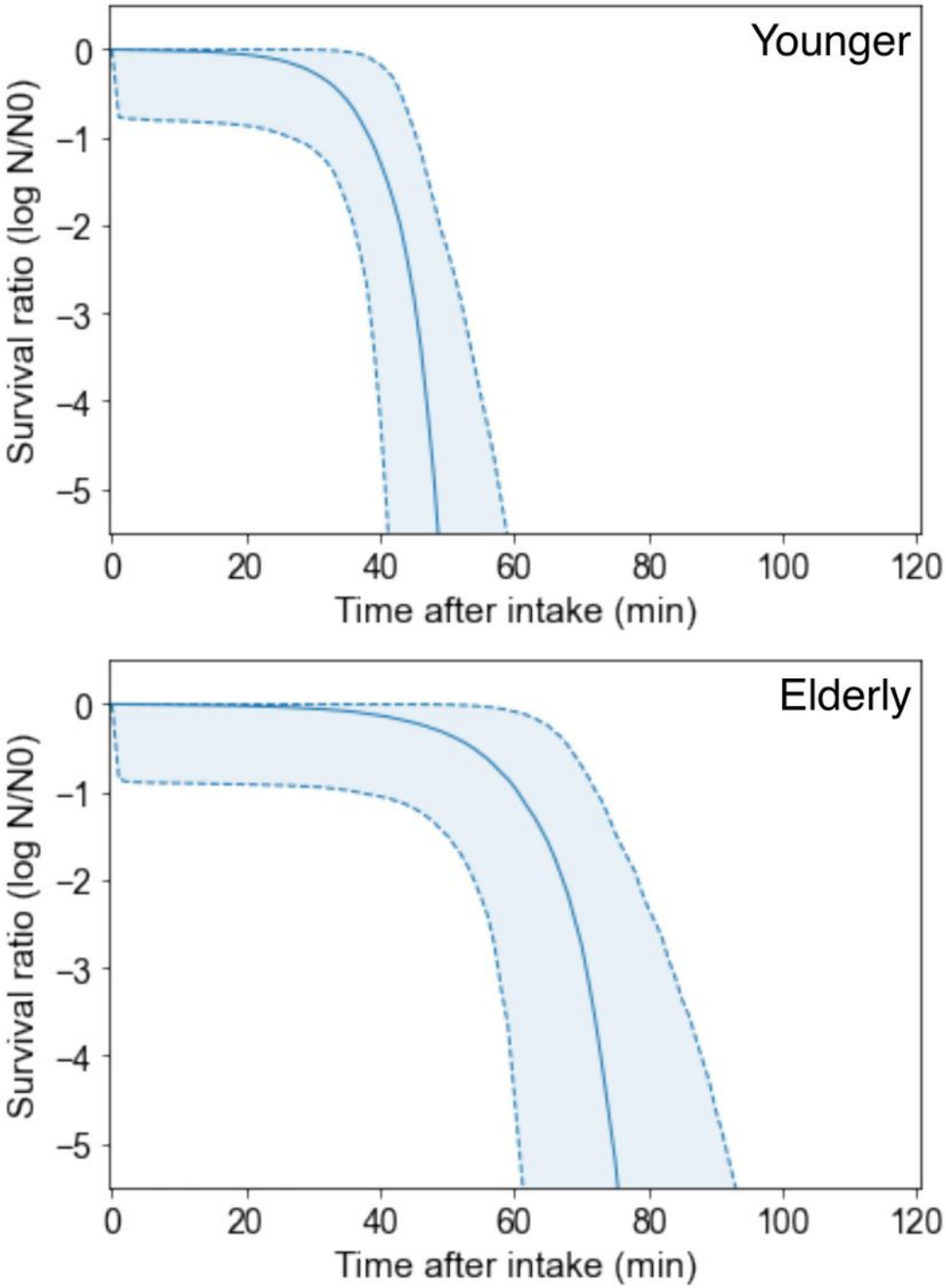

Figure 3

Predicted after-meal survival curves (solid curve: median, dash curve and covered range: 90% prediction band) of C. jejuni in the stomach of young (upper) and elderly (lower) people.

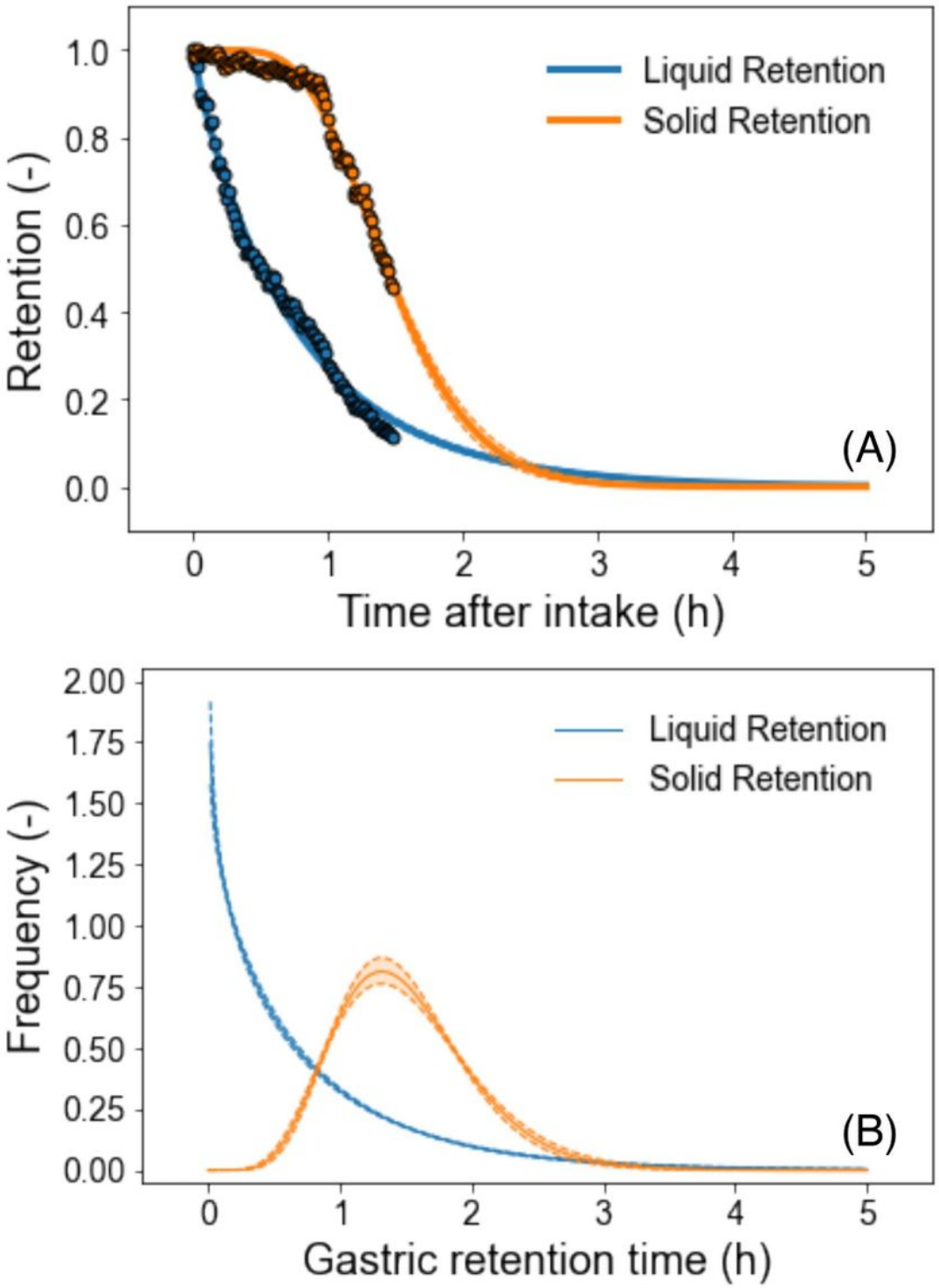

Figure 4

Reported retention ratio (a; points) & predicted cumulative gamma distributions (a and b; solid curve: median, dash curve and covered range: 95% prediction band) for gastric retention time (Appendix: Estimated parameter distribution of retention models).

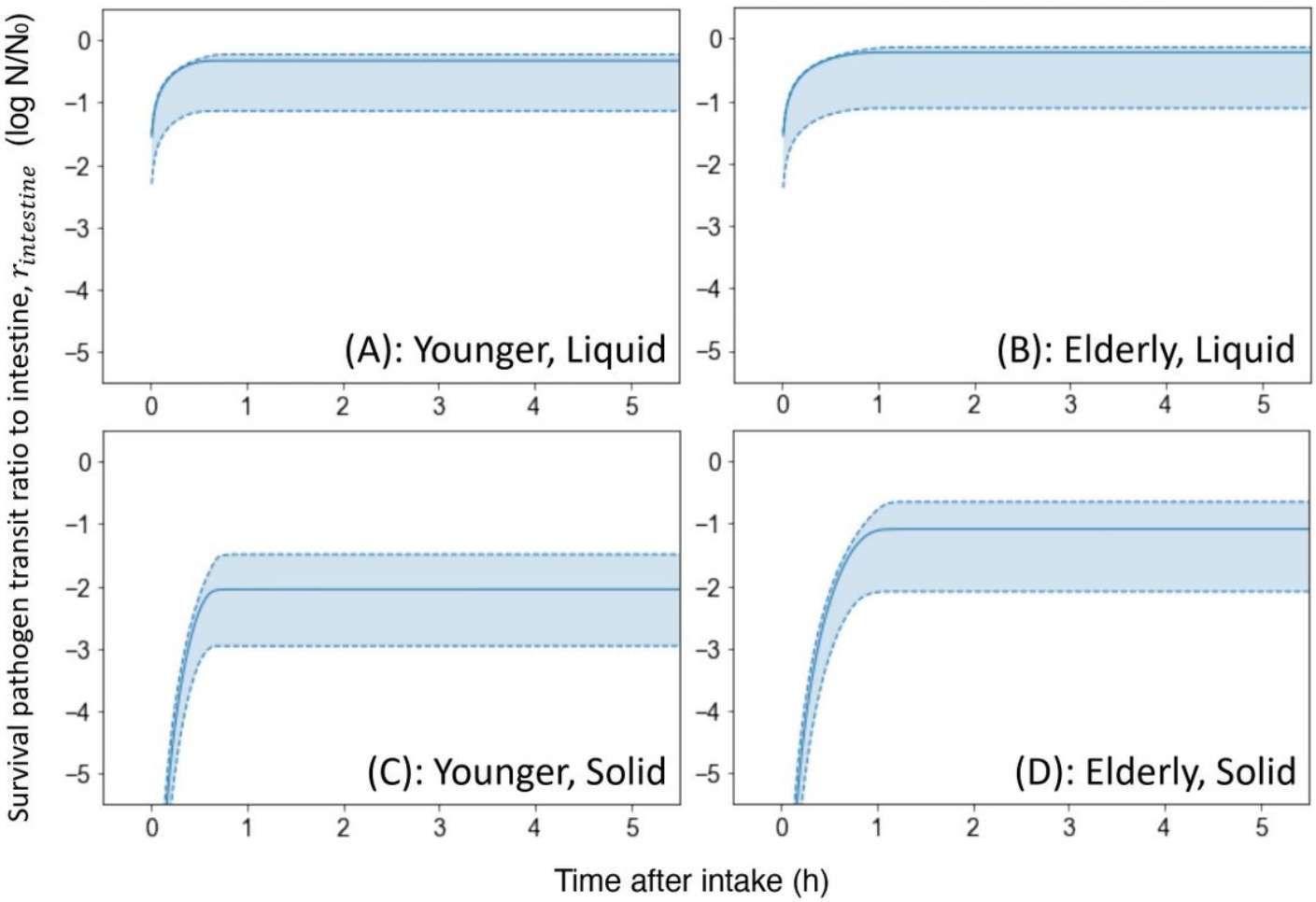

Figure 5

Calculated transferred survival ratio (solid curve: median, dash curve and covered range: 90% prediction band) in intestine under each condition (a: young and liquid food, b: elderly and liquid food, c: young and liquid food, d: elderly and solid food).

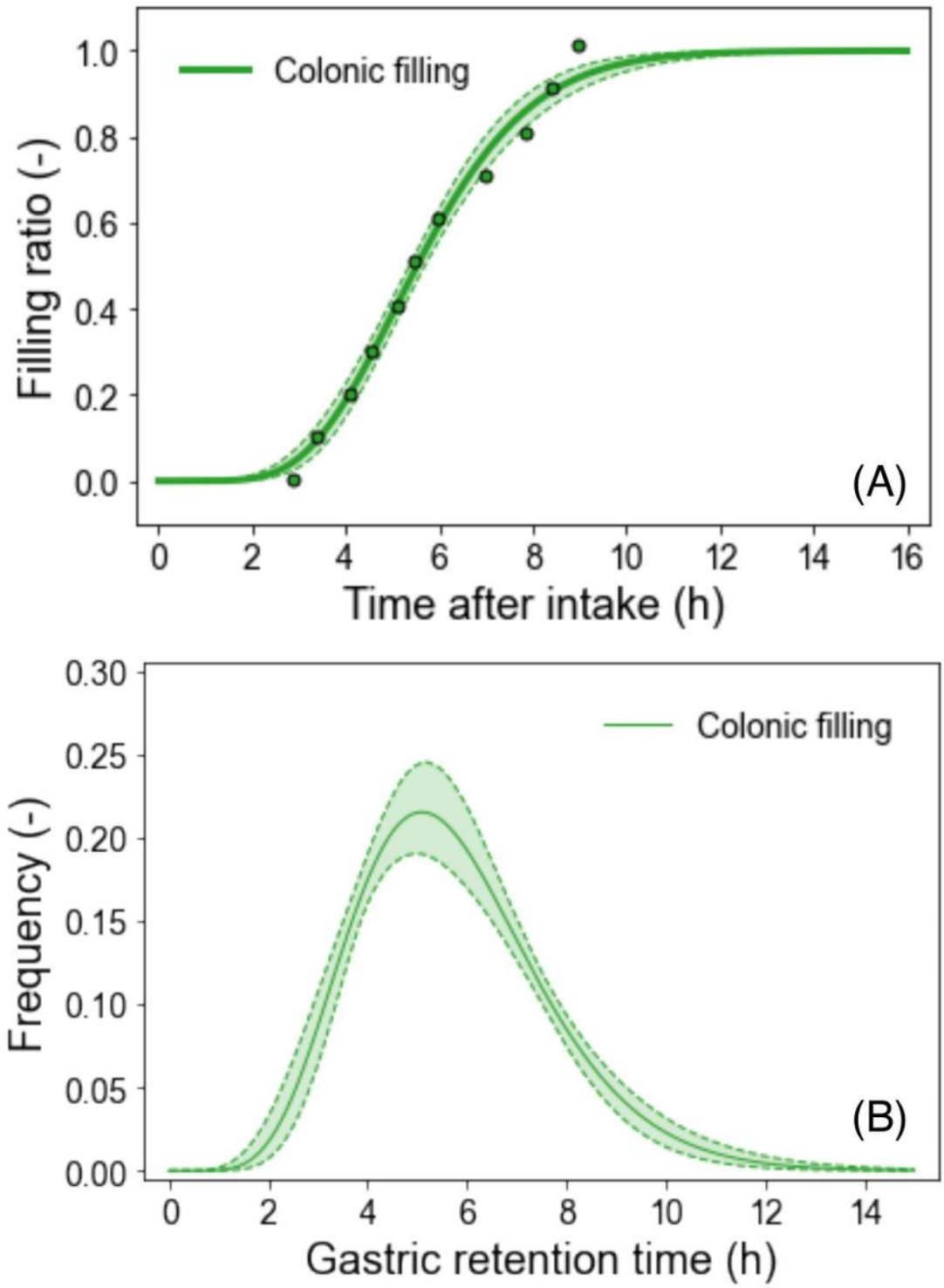

Figure 6

Reported colonic filling ratio (a; points) and predicted cumulative gamma distribution for retention time in small intestines (a and b; solid curve: median, dash curve and covered range: 95% prediction band). (Appendix Estimated parameter distribution of colonic filling)

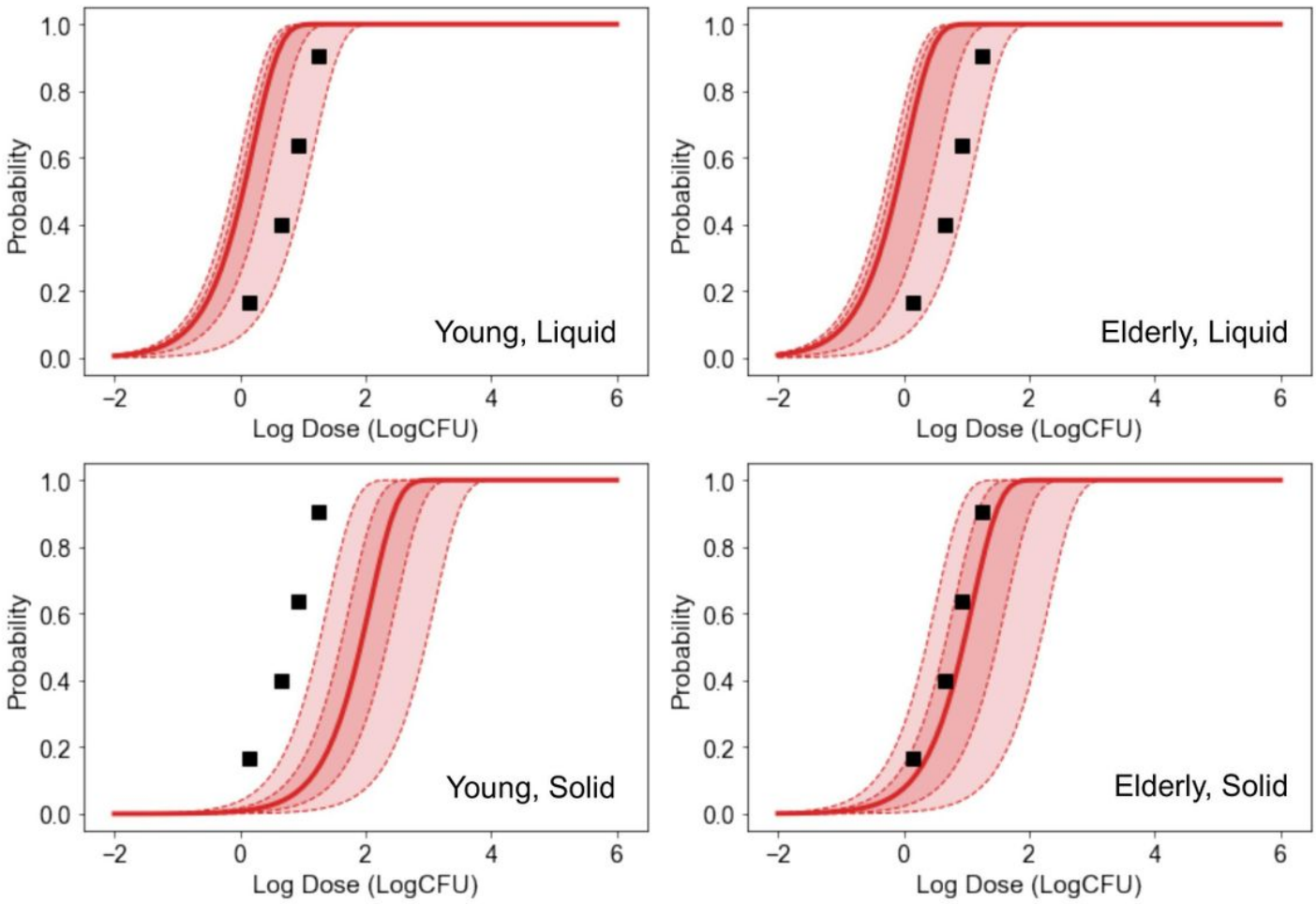

Figure 7

Cell invasion probability (solid curve: median, dash curve and covered range: 60% and 95% prediction band) of C. jejuni (total of all three strains) under each condition (Same position as Fig. 5) and the reported dose-response relationship (square; Teunis et al., 2005)

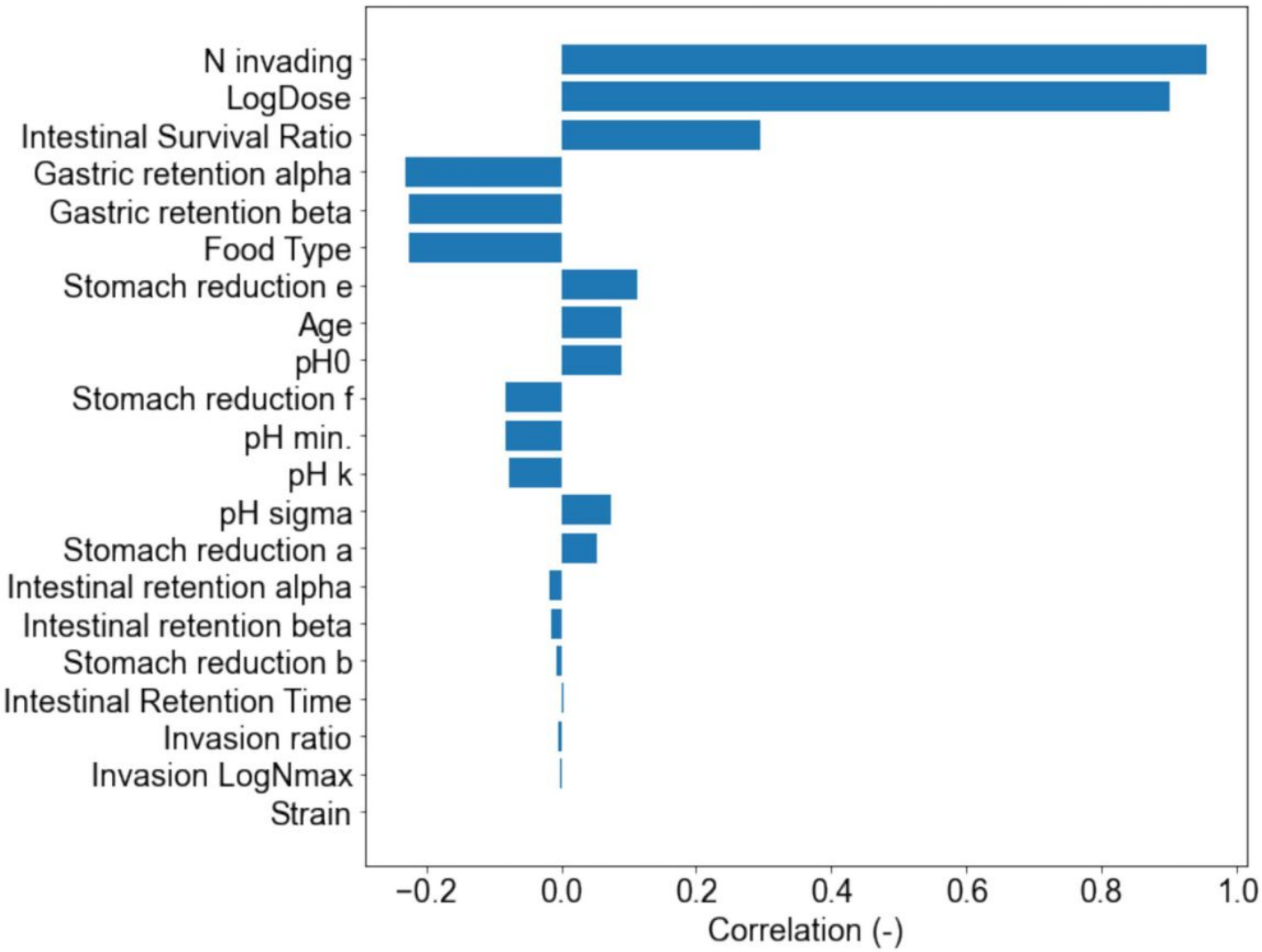

Figure 8

Spearman's ranked correlation coefficients of parameter and computable factors against the predicted infection probability.

Supplementary Files

This is a list of supplementary files associated with this preprint. Click to download.

- Supplementaryinformation.docx